https://doi.org/10.5194/os-2019-123
Preprint. Discussion started: 9 December 2019

Ocean Science
Discussions

Circulation of the European Northwest Shelf: A Lagrangian perspective

Marcel Ricker[1*] and Emil V. Stanev[2]

[1]University of Oldenburg, Institute for Chemistry and Biology of the Marine Environment, Carl-von-Ossietzky-Straße 9-11, 26111 Oldenburg, Germany

[2]Institute of Coastal Research, Helmholtz-Zentrum Geesthacht, Max-Planck-Straße 1, 21502 Geesthacht, Germany

*Corresponding author: E-mail: marcel.ricker@uni-oldenburg.de

https://doi.org/10.5194/os-2019-123
Preprint. Discussion started: 9 December 2019

Ocean Science
Discussions
Open Access

Abstract

The dynamics of the European Northwest Shelf (ENWS), the surrounding deep ocean, and the continental slope between them are analysed in a framework of numerical simulations using Lagrangian methods. Several sensitivity experiments are carried out in which (1) the tides are switched off, (2) the wind forcing is low-pass filtered, and (3) the wind forcing is switched off. To measure particle accumulation, a quantity named the "density trend" is introduced. Yearly averages of the results in the deep ocean show no permanent particle accumulation areas at the surface. On the shelf, elongated accumulation patterns persist on yearly time scales, often occurring along the thermohaline fronts. In contrast, monthly accumulation patterns are highly variable in both regimes. Tides substantially affect the particle dynamics on the shelf and thus the positions of fronts. The contribution of wind to particle accumulation in specific regions is comparable to that of tides. The role of vertical movements in the dynamics of Lagrangian particles is quantified both for the eddy-dominated deep ocean and for the shallow shelf. In the latter area, winds normal to coasts result in upwelling and downwelling and very clear patterns characterising the accumulation of Lagrangian particles associated with the vertical circulations.

https://doi.org/10.5194/os-2019-123
Preprint. Discussion started: 9 December 2019

Ocean Science Discussions
Open Access EGU

1 Introduction

The European Northwest Shelf (ENWS) (Fig. 1) is among the most studied ocean areas worldwide. Numerous reviews have presented details of its physical oceanography (e.g. Otto et al., 1990; Huthnance, 1991 Understanding the dynamics of the ENWS has been achieved considerably through numerical modeling (Maier-Reimer, 1977; Backhaus, 1979; Heaps, 1980; Davies et al., 1985; Holt and James, 1999; Pohlmann, 2006; Zhang et al., 2016; Pätsch et al., 2017). In contrast, the usefulness of Lagrangian methods for better understanding the ENWS dynamics has not been widely investigated heretofore.

In the following, we briefly summarize some basic oceanographic knowledge about the ENWS (the study area is shown in Fig. 1). The slope current dynamics and exchanges between the deep ocean and shelf have been analysed by Huthnance (1995), Davies and Xing (2001), Huthnance et al. (2009) and Marsh et al. (2017); Lagrangian drifter experiments in this area have been described by, e.g. Booth (1988) and Porter et al. (2016). The prevailing westerlies induce on-shelf water transport from the Celtic Sea up to the Outer Hebrides (Huthnance et al., 2009). Water entering the Celtic Sea flows either into the English Channel or into the Irish Sea via St. George's Channel. The water exiting the Irish Sea flows around the Outer Hebrides and joins the on-shelf transported water. Part of this water enters the North Sea, mainly via the Fair Isle Current, where it begins an anti-clockwise journey through the North Sea. The third path of waters entering the North Sea originates from the Baltic, following which those waters are integrated into a complex system of currents in the Skagerrak and the Norwegian Trench. In this area, the Atlantic and Baltic Sea waters undergo strong mixing. Along the southern slope of the Norwegian Trench, a branch of the European Slope Current flows toward the Baltic Sea, while a current flowing in the opposite direction follows the northern slope of the trench. In addition, large river runoff influences the water masses in the North Sea and along the Scandinavian coast, explaining the low salinity along coastal areas. The major hypothesis in the present study is that although the North Sea is very shallow, it contains an important vertical circulation. Revealing such characteristics is the first objective of the present study.

https://doi.org/10.5194/os-2019-123
Preprint. Discussion started: 9 December 2019

Ocean Science
Discussions
Open Access

Much is known about the thermohaline fronts on the ENWS and its estuaries (Simpson and Hunter, 1974; Hill et al., 2008; Holt and Umlauf, 2008; Pietrzak et al., 2011). Although large parts of this ocean area are vertically well mixed, seasonal and shorter-term variability lead to pronounced differences in the positions and strengths of the fronts; freshwater fluxes are also important, particularly in shallow coastal areas. Krause et al. (1986), Le Fèvre (1986), Belkin et al. (2009), Lohmann and Belkin (2014), Mahadevan (2016) and McWilliams (2016) addressed the biological consequences of frontal systems, and the frontal physics are summarized in Simpson and Sharples (2012). However, to the best of the authors' knowledge, the frontal dynamics of the ENWS have not been addressed from a Lagrangian perspective, which constitutes the second objective of our study.

Most previous studies that employed Lagrangian particle tracking in the region of the ENWS (Backhaus, 1985; Hainbucher et al., 1987; Schönfeld, 1995; Rolinski, 1999; Daewel et al., 2008; Callies et al., 2011; Neumann et al., 2014 and Marsh et al., 2017) addressed only part of the region studied herein. Hence, our third objective is to provide a comparison among the specific hydrodynamic regimes in different areas of the ENWS and exchanges between these areas. One example has been recently provided by Marsh et al. (2017) for part of the European Slope Current.

The present study was initiated in the framework of a project studying the fate of marine litter in the North Sea (Gutow et al, 2018; Stanev et al, 2019). Here, we extend the area of our analyses to include the entire ENWS, the European Slope Current, the Bay of Biscay and parts of the Northeast Atlantic. Unlike our recent studies, herein, we address Lagrangian particles transported by 3-D ocean currents (Stokes drift and wind drag are not considered). Lagrangian approaches applied to the study of other ocean regions can be found in, e.g. Bower et al. (2009) for the North Atlantic, Paparella et al. (1997) for the Antarctic Circumpolar Current, Reisser et al. (2013) for Australia, van Sebille et al. (2015) for the world ocean, Maximenko et al. (2018) for tsunamis, Froyland et al. (2014) and van der Molen et al. (2018) in terms of connectivity studies.

https://doi.org/10.5194/os-2019-123
Preprint. Discussion started: 9 December 2019

Ocean Science
Discussions
Open Access
EGU

In Sect. 2, we will describe the model, its setup, the simulated dynamics and the Lagrangian experiments. In Sect. 3, our results are presented and discussed. The paper ends with a brief conclusion and an outlook in Sect. 4.

2 Materials and methods

2.1 The numerical model

The Nucleus for European Modelling of the Ocean (NEMO) hydrodynamic ocean model is used in this paper (https://www.nemo-ocean.eu/; Madec, 2008). For this study, the Atlantic Margin Model configuration with a 7 km resolution (AMM7; Fig. 1) of NEMO is chosen because it appears to be one of the best validated models for the ENWS (O'Dea et al., 2012 and 2017). The numerical model solves the primitive equations using hydrostatic and Boussinesq approximations. The horizontal resolution is $^1/_9$° in the zonal direction and $^1/_{15}$° in the meridional direction; that is, the resolution is approximately 7.4 km. There are 297 × 375 grid points altogether and 51 vertical σ-layers. For tracer advection, we employ the total variation diminishing (TVD) scheme, diffusion takes place on geopotential levels with a Laplacian operator (the horizontal eddy diffusivity is specified as 50 $m^2\ s^{-1}$). For momentum diffusion, a bi-Laplacian scheme is applied to act on the model levels (horizontal eddy viscosity = $-1\cdot10^{10}\ m^4\ s^{-1}$). The generic length scale (GLS) k-ε scheme is used as the turbulence closure scheme; the bottom friction is nonlinear with a log-layer structure and a minimum drag coefficient of $1\cdot10^{-3}$. The baroclinic time step is 300 s. The output, including the salinity (S), temperature (T), velocities (u, v) and sea surface height (SSH), is written hourly.

The atmospheric forcing is provided by the UK Met Office atmospheric model with a 3-h temporal resolution for the fluxes and an hourly resolution for the 10-m wind and air pressure. The model uses climatological river runoff, and tidal forcing is prescribed at the open boundary. The period of integration considered here spans from 01 January 2014 to 31 December 2015 of which the first year is the spin-up period. The analyses of the results are performed for the area between 42.57° N–63.50° N and 17.59° W–13.00° E.

https://doi.org/10.5194/os-2019-123
Preprint. Discussion started: 9 December 2019

Although part of this study could be performed using the freely available Forecasting Ocean Assimilation Model (FOAM) AMM7 data (https://marine.copernicus.eu), we run the abovementioned model to (1) perform Lagrangian simulations online and (2) carry out some additional sensitivity experiments. In contrast to the operational AMM7 model, the data are not assimilated here. In the following, the basic experiment is referred to as the control run (CR). In one sensitivity experiment, the tides are turned off; this experiment is referred to hereafter as the nontidal experiment (NTE). In two other sensitivity experiments, the wind forcing is low-pass filtered with a moving time window of one week (referred to as the filtered-wind experiment, FWE) or completely turned off (the nonwind experiment, NWE).

2.2. Model velocity validation

The velocities of the CR have been validated using 9 passive GPS surface drifters; these drifters provide the most appropriate type of in situ data for validating the model's ability of particle advection. The drifters, which have a bottom-mounted sail to reduce direct wind drag, were designed to be moved by the upper 1 m of the ocean. The drifters were released in the German Bight during RV *Heincke* cruise HE445, and their position was sent every ~20 minutes from May to July 2015. The dataset is freely available (Carrasco and Horstmann, 2015). To the best of the authors' knowledge, this is the only GPS drifter dataset available for the ENWS during the period of the simulations analysed herein. For validation, the model velocities are interpolated to the drifter positions in space and time and compared against the drifter velocities. The corresponding scatter plots (Fig. S1a and S1b) show a good model performance in the range of ±25 cm s^{-1}, where the quantile-quantile plot (qq-plot) is almost along the diagonal. Deficiencies in the model occur at higher velocities, where the model is too slow. Nevertheless, the linear correlations of the u and v velocity components of 0.89 and 0.85, respectively, between the drifters and the model and the corresponding root mean square errors (RMSEs) of 13.9 and 12.2 cm s^{-1} are considered to reflect a satisfactory model performance (Table 1).

The quality of the above numbers illustrating the model skill can be better understood if the drifter data are compared with independent observations; in the following, a comparison is performed with HF

https://doi.org/10.5194/os-2019-123
Preprint. Discussion started: 9 December 2019

radar data. The HF radar system described by Stanev et al. (2015) and Baschek et al. (2017) consists of 3 measurement stations covering most of the German Bight and measures ocean surface velocities. These data are freely available (http://codm.hzg.de/codm/). The corresponding scatter plots (Fig. S1c and S1d) do not show as much underestimation of high velocities as in the model (compare with Fig. S1a and S1b), but the spread of the data in two observations is comparable to the case of the model-data comparison (the standard deviation between the two observations is even larger than in the case of the model-data comparison). The conclusion from Table 1 is that the difference between the estimations from the model and data are not larger than that between two observations. Similar validations provided by Stanev et al. (2019) for the North Sea also demonstrate the credibility of the Lagrangian tracking approach.

Table 1: Summary of the model validation performed by comparing GPS drifter velocities with the CR and HF radar velocities; the surface velocity components of the latter were interpolated to the drifter velocities. Details are given in the text. A positive bias denotes that drifter velocities are larger than the velocities of the CR or HF radar. The corresponding scatter plots are given in Fig. S1.

	Drifter - CR		**Drifter - HF radar**	
	u	v	u	V
RMSE [cm s^{-1}]	13.9	12.2	18.4	12.5
Linear correlation	0.89	0.85	0.91	0.87
Standard deviation [cm s^{-1}]	13.7	12.1	16.9	12.4
Bias [cm s^{-1}]	2.7	1.3	7.4	-2.0

2.3. Analysis of the simulated dynamics

The circulation of the CR is very diverse in different model areas, but the differences among the dynamic regimes in the CR are most pronounced between the deep ocean and the shelf. The averaged velocities and velocity amplitudes (U) for January 2015 (Fig. 2a and 2b) show basically two regimes: an eddy-dominated regime west of the continental slope and a tidally dominated regime on the shelf. The latter is characterized by relatively low mean velocities (Fig. 2a) and large velocity oscillations in the English Channel (Fig. 2b). The transition between these two regimes occurs along the 200 m isobath (Fig. 2a), which can be considered a separation line between the dynamics of the shelf and deep ocean.

https://doi.org/10.5194/os-2019-123
Preprint. Discussion started: 9 December 2019

A sequence of mesoscale eddies is developed offshore of the western shelf edge with a dominant one in the Rockall Trough (Fig. 2a and 2b), which are also readily visible in the corresponding SSH pattern (not shown). The largest amplitudes of the sea level oscillations are observed around the British Isles and along the southern coasts of the German Bight.

The simulated thermohaline characteristics are consistent with the existing knowledge: the coastal waters, particularly those in the German Bight, are less saline (Fig. 2c) and represent typical regions of freshwater influence (ROFIs). In the German Bight, most of the low-salinity water originates from the Rhine, Ems, Weser and Elbe Rivers and spreads along the Dutch, German and Danish coasts before it reaches the Skagerrak, where it mixes with the low-salinity outflow from the Baltic Sea. The pattern of the salinity gradient (Fig. 2d) reveals features along the coasts, in the Norwegian Trench and at the major fronts in the German Bight and Norwegian Trench.

In the winter, the overall temperature distribution is characterized by cold temperatures on the shallow shelf and a south-north temperature gradient in the deep water south of Ireland (Fig. 2e). A warm water plume exits the English Channel and traces the pathway of warm Atlantic water in the North Sea, which is also known from the satellite observations of Pietrzak et al. (2011). The East Anglia Plume and the Frisian Front are promptly visible as low-temperature areas originating from the East Anglia coast (Fig. 2e). The two current branches in the Norwegian Trench associated with the two opposing flows (one flowing to the east along the southern slope and another flowing in the opposite direction along the northern coast) are also easily observed as areas characterised by large temperature gradients (Fig. 2f) coinciding with the salinity gradient maximum; a number of mesoscale features occur in the deep ocean along the rims of currents (compare with Fig. 2a). In the summer, the warmest temperatures can be found on the shallow shelf, especially on the Armorican Shelf (Fig. S2a). The summer temperature distribution is also characterized by well-pronounced temperature gradients. The simulated gradients along the Celtic Sea Front, Ushant Front, Islay–Malin Head Front and the Flamborough Head Front (black circles in Fig. S2a) support the results of Pingree and Griffiths (1978). The disappearance of some of these fronts in the results of the NTE demonstrates that they are tidal

https://doi.org/10.5194/os-2019-123
Preprint. Discussion started: 9 December 2019

Ocean Science
Discussions
Open Access

mixing fronts (see Fig. S2a and S2b). Overall, Fig. 2 supports much of what is known from previous studies (e.g. Pätsch et al., 2017).

Understanding the differential properties of currents is of utmost importance to understand the propagation of tracers. Therefore, we will present a brief analysis of deformation, as proposed by Smagorinsky (1963):

$$|D| = \sqrt{{D_T}^2 + {D_S}^2} = \sqrt{\left(\frac{\partial u}{\partial x} - \frac{\partial v}{\partial y}\right)^2 + \left(\frac{\partial u}{\partial y} + \frac{\partial v}{\partial x}\right)^2} \quad (1)$$

with horizontal tension strain

$$|D_T| = \sqrt{\left(\frac{\partial u}{\partial x} - \frac{\partial v}{\partial y}\right)^2} \quad (2)$$

and horizontal shearing strain

$$|D_S| = \sqrt{\left(\frac{\partial u}{\partial y} + \frac{\partial v}{\partial x}\right)^2}\,. \quad (3)$$

Figure 2g shows the 25-h averaged deformation obtained from the CR surface currents. The order of this property $O\,(10^{-5})$ is within the ranges measured by Molinari and Kirwan (1975) with Lagrangian drifters. The most obvious features are the two large areas on the shelf exhibiting low deformation, namely, the North Sea and the Celtic Sea, including the Armorican Shelf connected by the English Channel and Southern Bight, where several localized high-deformation areas appear (compare Fig. 2g with 2b). High-deformation areas are also present in the Irish Sea extending to the northern coast of Ireland. The difference between the CR and NTE clearly shows the effects of tides on the deformation in these three areas (Fig. 2h). Despite these shallow, enclosed areas, the deformation along the shelf edge of the Celtic Sea is also affected by tides. High-deformation features in the deep ocean arise at the

https://doi.org/10.5194/os-2019-123
Preprint. Discussion started: 9 December 2019

eddy boundaries (compare Fig. 2g with 2a) and are also present in the NTE; hence, flow deformation is expected to be of significant importance for water masses in the deep ocean. Exceptions are the Bay of Biscay and the northwest of the domain where the deformation is less pronounced in the NTE. The difference patterns there have scales of mesoscale eddies suggesting that these eddy dynamics could be coupled to the one of tides. In the Norwegian Trench, the influence of tides on deformation is strong due to the small-scale dynamics associated with the two currents along the north and south topography slopes and the eddies between them.

2.4 Particle release experiments

Lagrangian particles are released in the hydrodynamic model, and their propagation is used to analyse the transport properties. The experiments were carried out "online"; that is, the particle trajectories were computed within the hydrodynamic model at every time step. Additional experiments were carried out "offline" using the model velocity output. High-frequency processes and vertical transport are better accounted for in the former experiments. This intercomparison between the online and offline integrations demonstrates that neither approach leads to drastic differences when comparing 2-D particle transport properties.

The online advection of Lagrangian particles was achieved by the freely available open-source ARIANE model (http://stockage.univ-brest.fr/~grima/Ariane/). The version of ARIANE implemented in NEMO has frequently been used in other studies, e.g. Blanke and Raynaud (1997) and Blanke et al. (1999). Further details of the ARIANE model can be found in the appendix of Blanke and Raynaud (1997) and in the ARIANE user manual. Beaching is not possible; that is, the total number of particles remains constant over time. An extra wind drag is not used, nor is additional horizontal diffusion for the particles, because it is assumed that the high temporal resolution of the velocity fields and large velocity gradients will provide a sufficiently high diffusivity (van Sebille et al., 2018). The vertical velocity is taken into account, and the particle positions are written hourly.

https://doi.org/10.5194/os-2019-123
Preprint. Discussion started: 9 December 2019

Ocean Science Discussions
Open Access
EGU

Different seeding strategies were implemented. In one class of experiments (#1 and 4–6 in Table 2), the particles were seeded at 1 m (surface particles), as well as in the grid cells just above the seafloor (bottom particles). In the second experiment (#2 in Table 2) named CR-V, particles were released in a 100 km wide stripe extending oceanward from the 150 m isobath starting in the Bay of Biscay and ending north of the Shetland Islands at 61.7° N; in this experiment, particles were seeded vertically every 20 m. In a third experiment (#3 in Table 2) named CR-B, the particle tracking process was carried out offline; for this purpose, the freely available open-source model OpenDrift (Dagestad et al., 2017) was used, in which the particles were advected by a 2nd-order Runge–Kutta scheme. The offline calculation was performed backward in time at a constant depth with a velocity input time step, a model time step and an output time step of 1 h. The particle release depth in this experiment was 1 m.

The seeding strategy was consistently executed as follows. The initial distribution of particles was uniform with 1 particle per model grid cell, that is, 64,831 particles per depth layer for the whole domain (experiments #1 and 3–6 in Table 2) and a total of 345,011 particles in experiment #2. In the CR and CR-V (experiments #1 and 2, respectively), particle release was repeated on the first day of every month in 2015, and particles were traced for 1 month. Thus, 12 data sets, each including 1 month of trajectory data, were generated. Additionally, for the seeding in January, the particle positions were saved for 6 months. The CR-B, FWE and NWE (experiments #3, 5 and 6, respectively) were conducted only for January 2015; the NTE (experiment #4) was further performed for July 2015.

Table 2: Summary of the particle release experiments; further details are given in Sect. 2.4.

# (abbr.)	Particle advection		Spatial seeding			Integration time	Details
	Online	Offline	Whole domain	Shelf edge	Vertical		
1 (CR)	x		x		surface & bottom	12 x 1 month	3-D particle motion
2 (CR-V)	x			x	every 20 m	12 x 1 month	3-D particle motion
3 (CR-B)		x	x		surface	January	backtracking
4 (NTE)	x		x		surface & bottom	January + July	no tides
5 (FWE)	x		x		surface & bottom	January	filtered wind
6 (NWE)	x		x		surface & bottom	January	no wind

https://doi.org/10.5194/os-2019-123
Preprint. Discussion started: 9 December 2019

2.5 Particle density trend

The analyses of the results will focus on typical Lagrangian properties, e.g. the positions of the particles and their trajectories. Such a presentation could be considered inferior compared with the Eulerian presentation, which displays the concentrations of properties. However, from these Lagrangian characteristics, one can derive properties similar to the concentration that can represent the "compaction" process of particles in certain areas or identify the areas that are more frequently visited by the Lagrangian particles. These properties related to particle density allow the areas in which particles accumulate to be identified.

Different approaches to quantify particle accumulation have been proposed (Koszalka and LaCasce; 2010; Koszalka et al., 2011; van Sebille et al., 2012; Huntley et al., 2015). Below, in addition to the typical Lagrangian properties, a property named the "density trend (DT)" is introduced that measures the number of particles that have visited each grid cell during a certain time interval. This quantity is normalised by the corresponding number of particles in the motionless situation for the same time interval, in our case, 1 particle per grid cell:

$$DT(x, y, t_n) = \frac{\sum_{i=0}^{n} N_{u\neq 0}(x, y, t_i)}{\sum_{i=0}^{n} N_{u=0}(x, y, t_i)} \tag{4}$$

where *DT* is the density trend, (x, y) are the coordinates of an arbitrary grid cell with dimensions (dx, dy), n is the number of time steps from t_0 to t_n, u is the velocity field and N is the number of particles at time step i in grid (x, y). In the present study, (dx, dy) represent the model grid dimensions but could be larger or smaller for other applications. A DT greater (smaller) than unity corresponds to more (fewer) particles, which are identified in a grid cell on average, than there would be without currents. Thus, the DT can be interpreted as the percentage of the initial number of particles averaged over time.

The definition of the DT is not straightforward if the initial particle concentration is zero in some areas. If the number of particles in some areas remains small (e.g. areas close to an inflow-dominated

https://doi.org/10.5194/os-2019-123
Preprint. Discussion started: 9 December 2019

open boundary or divergence zones), the statistical confidence of this property cannot be ensured. Therefore, areas where the DT is less than 30 % are excluded from the analysis (white areas in the following figures). Overall, for integration times longer than 1 month, large areas remain free of particles; thus, t_n is chosen to be 1 month in the present study.

3 Results and discussion

3.1 Overall analysis of trajectories and particle dynamics

The particle trajectories (Fig. 3) of the CR (experiment #1, see Table 2) show the well-known, dynamic features of the ENWS and the surrounding deep ocean. In relatively shallow areas, e.g. the English Channel, Southern Bight and Irish Sea, the surface and bottom currents reveal similar patterns, which is typical for wind-driven shallow water circulation (Fig. 3a and 3b). Trajectories symbolising currents appear relatively thick in the areas dominated by strong tides because the large-scale presentation cannot effectively resolve small tidal excursions. This is supported by the magnified representation of the dynamics in Fig. 3c and 3d. After 12 h, the trajectories on the shelf present as nearly closed circles. The difference between the start and end positions on the circular loops denotes the net transport, which is much smaller than the tidal excursions. The net transport rapidly increases, and the tidal excursions decrease further off-shelf beyond the 900 m isobaths, where the mesoscale dynamics are dominant. As in the case of the Eulerian visualisation of the velocity field, the 200 m isobath can be considered the boundary separating the dynamics of the shallow and deep ocean. The meandering of the European Slope Current along the shelf edge (at ~500–2,000 m) is pronounced from the Bay of Biscay to the Goban Spur and around the Porcupine Bank (Fig. 3b). The Skagerrak and Norwegian Trench also show pronounced mesoscale dynamics (Fig. 3d).

3.2 Tendencies of particle accumulation

3.2.1 Surface and bottom patterns of the particle distribution

Despite some similarities between the surface and bottom trajectories (Fig. 3), the particle accumulation patterns in shallow areas are considerably different. To investigate these differences, the positions of the particles released in January (CR, experiment #1, see Table 2) are displayed in Fig. 4. In the

https://doi.org/10.5194/os-2019-123
Preprint. Discussion started: 9 December 2019

Ocean Science Discussions
Open Access
EGU

following, "+" and "-" symbols will be used to denote locations of particle accumulation ("+") and removal ("-"). After 1 month, the surface-released particles accumulate mainly along narrow patterns on the shelf and in the Skagerrak (Fig. 4a). In contrast, the coastal regions around Great Britain and Ireland (but also in the German Bight) can be considered divergence zones. The particle distribution in the deep ocean also shows small stripe-type patterns, especially in the southwestern part of the model domain.

There is a tendency for the bottom-released particles to leave areas with a steep bottom slope. The most obvious example is the continental slope are along the 200 m isobath from the Spanish coast around the Goban Spur and Porcupine Bank (Fig. 4b) until the Norwegian Trench. Van Aken (2001), Huthnance et al. (2009) and Guihou et al. (2018) demonstrated that slope currents, downward flows of shelf water and breaking internal waves, respectively, dominate the dynamics of the ENWS continental slope. Thus, this tendency of bottom-released particles to leave the continental slope is consistent with the findings of earlier studies on the dynamics of the ENWS shelf edge.

After 6 months, vast areas of the shelf and the western part of the domain become free of particles. The Lagrangian particles flow from the English Channel along the Frisian Front in the south and the Fair Isle Current in the north into the inner North Sea (Fig. 4c). The pattern in the Irish Sea is similar to the Frisian Front: a narrow stripe of particles in the middle of this basin is the remnant of a similar stripe from an earlier time (Fig. 4a) connecting the source of particles (in the south) to their sink (in the north). The region around the Orkney and Shetland Islands accumulates particles owing to on-shelf transport by the westerlies. This region additionally receives particles from the south originating from the Irish Sea or having flown around the western coast of Ireland; in both cases, these particles are sourced from the deep ocean. Bottom accumulation on the shelf occurs mainly south of the Dogger Bank (Fig. 4d). Also the bottom trajectories (Fig. 3b) show that particles north of Dogger Bank are forced to flow around its western edge through a narrow channel into the basin to its southeast (see the bathymetry in Fig. 1) suggesting topographically influenced particle motions. Once the particles reach this basin, they

https://doi.org/10.5194/os-2019-123
Preprint. Discussion started: 9 December 2019

can flow out only northward along its thalweg until they reach the northeastern edge of Dogger Bank (compare Fig. 4d with Fig. 1).

In the Skagerrak, the situation is as follows. At the bottom, the Norwegian Trench supplies the Skagerrak with particles from the Atlantic along its southern slope. At the surface, the Skagerrak receives particles from the German Bight and the Baltic Sea. Particles approaching the Skagerrak can become trapped in its circular and eddy-dominated velocity pattern (Fig. 3d and 2b), which extends from the surface down to the bottom (see also Rodhe, 1987; Gutow et al., 2018). In the Norwegian Trench, the particle distribution is ambiguous due to the irregular mesoscale dynamics therein.

The current particle positions are not sufficiently representative of their accumulation and dispersal over long periods and can lead to misinterpretations of their accumulation trends. This becomes evident by comparing the particle positions after 1 month (Fig. 4a and 4b) with the DT for the same period (Fig. 5a and 5b). Although the general surface and bottom patterns (Fig. 4a and 4b) for January 2015 are comparable to the mean accumulation patterns (Fig. 5a and 5b), some features do not coincide. The monthly DTs for all twelve months are shown in Figure S3 and S4 for the surface- and bottom-released particles, respectively. At the surface, only a few accumulation areas are visible on the annual mean map (red areas in Fig. 5c); these areas are located in the Irish Sea (*1*), English Channel (*2*), Southern Bight (*3*), German Bight (*4*), Skagerrak (*5*), along the continental slope (*6*), and at the Fair Isle Current (*7*). Vast coastal areas have a DT smaller than 0.3, implying off-coast propagation. Despite the numbered accumulation areas and coasts prone to particle removal, most of the domain shows neither particle accumulation nor removal (DT ≈ 1).

At the bottom, particle accumulation is rather ambiguous in the deep ocean, but the removal of particles from areas with steep topography is evident (Fig. 5d). On the shelf, the tendency of particles to propagate away from coasts is reduced; particles even accumulate, e.g. in the German Bight and along the eastern British coast (discussed in detail in Sect. 3.3). Further, accumulation takes place to

https://doi.org/10.5194/os-2019-123
Preprint. Discussion started: 9 December 2019

the south of Dogger Bank and in the Skagerrak. It is worth noting that the major accumulation pattern at the surface along the Frisian Front (*3*, *4*) has as its counterpart a pattern of removal at the bottom (compare Fig. 5c and Fig. 5d). Additionally, coastward of accumulation area *4*, there is a removal area at the surface; in the same area, the bottom pattern shows a tendency of accumulation. These opposite tendencies in the surface and bottom layers suggest that the vertical circulation is also important in shallow environments. The inflow along the southern slope of the Norwegian Trench appears as increased particle accumulation.

There are some prominent small-scale features (stripe-like or filament-like characteristics) occurring in the deep ocean (Fig. 5a and S3). These features change their positions depending on the eddy motion. They are reminiscent of the attributes reported by Haller and Yuan (2000), who demonstrated that particles initially located outside eddies accumulate in lines along the boundaries between them. When the averages are computed for a longer period, these filaments tend to disappear (compare Fig. 5a with 5c), which is explained by the fact that the time scales of eddy motions are substantially shorter than the annual scale. This follows from the changes in the position and occurrence of the stripe-type areas with DTs greater than 1 from month to month (compare the results from single months of Fig. S3). A more profound Lagrangian representation of eddies and their coherent character can be found in, e.g. Beron-Vera et al. (2018).

3.2.2 The role of tides

The difference in the January DTs between the CR and NTE (experiments #1 and 4, respectively, see Table 2 and Fig. 6a and 6b) demonstrates that the tidal forcing considerably affects the accumulation patterns on the shelf. The largest differences between the two experiments (marked with "***" symbols) occur along the Frisian Front and along the front in the Irish Sea (Fig. 6a and 6b). These differences show greater accumulation at the surface in the CR at the western flanks of these fronts and less accumulation at the eastern flanks than in the NTE. Obviously, the tidal signal affects frontal-like structures. Similar differences between the two experiments appear in the English Channel, around the

https://doi.org/10.5194/os-2019-123
Preprint. Discussion started: 9 December 2019

Ocean Science
Discussions

north of Great Britain, and at the continental slope of the Celtic Sea. In most of the remaining parts of the domain, these differences are rather small.

Nevertheless, tides also affect the accumulation of particles in the deep ocean, which is dominated by sub-basin-scale eddies, as well as other areas in the Bay of Biscay and in the Norwegian Trench/Skagerrak, which are dominated by mesoscale motions. This could serve as another indication of the interaction between tides and mesoscale dynamics.

The most pronounced large-scale feature in the differences observed at the sea surface is in the vicinity of the shelf (Fig. 6a). At the bottom (Fig. 6b), the largest differences between the two experiments occur beyond the 200 m isobaths in the direction of the open ocean. The changing sign of the difference reflects large oscillations at small scales, possibly indicating that a further increase in the model resolution is needed to adequately resolve the accumulation and dispersion of particles in the area of the continental slope. Bottom patterns in the North Sea are also present and clearly demonstrate the importance of tides as a driver of particle accumulation. The principal patterns are similar to the surface: around Great Britain the difference signal is rather ambiguous; in the Southern Bight and southern North Sea the difference patterns are rather distinct and follow the flanks of the East Anglia Plume and Dogger Bank. In the front itself, the tides do not have a significant impact on the accumulation of particles. This comparison between the surface and bottom patterns indicates that, unlike the currents, which do not drastically change in the vertical direction in the shallow ocean, the accumulation of particles at the bottom is different from that at the sea surface. This suggests that the current shear affected by tides modifies the particle accumulation patterns. This finding is supported by the influence of tides on deformation (compare Fig. 6a and 2h), the pattern of which partly coincides with the DT difference.

3.2.3 The role of wind

A large part of the variability is caused by atmospheric variability (mostly on synoptic time scales) (Jacob and Stanev, 2017); therefore, we will analyse the contributions of wind to the accumulation and

https://doi.org/10.5194/os-2019-123
Preprint. Discussion started: 9 December 2019

dispersion of particles in the FEW and NWE (experiments #5 and 6, respectively, see Table 2). It is worth noting that the ranges of the responses to wind are comparable to the responses to tides. The overall conclusion from the comparison among the differences in the surface properties between the CR and NTE (Fig. 6a) from one perspective and between the CR and FWE (Fig. 6c) from another perspective is that the largest differences caused by tides and winds occur in almost the same areas: the Frisian and Irish Sea Fronts, the continental slope, and the Norwegian Trench; the English Channel is less influenced in FWE. Smoothing the wind (FWE) makes the accumulation stripes "sharper", whereas the short-term wind forcing tends to "blur" the particle distribution. However, turning the wind off (NWE) changes the accumulation patterns significantly (compare Fig. 6e and 6c). The most affected areas are (1) the coastal areas of Great Britain and Ireland, (2) the Skagerrak, which no longer accumulates particles, (3) the mouths of the Rhine and Elbe rivers which extend further to the west, and (4) the accumulation area along the Celtic Sea shelf edge that disappears in the NWE. Reducing the variability of the wind or turning it off completely also has very pronounced impacts on the bottom particles (compare Fig. 6d and 6f). The accumulation patterns at the bottom are mostly affected in the northern part of the shelf and the Norwegian Trench/Skagerrak.

The difference between the FEW and NEW (not illustrated here) demonstrates that, on the shelf, the westerlies are essential for particle accumulation.

3.2.4 The role of fronts

The high-salinity and high-temperature gradients (fronts) in Fig. 2d and 2f are similar to the DT patterns shown in Fig. 5a. These fronts support the ones reported by Belkin et al. (2009), particularly the fronts in the southern North Sea. Additionally, in terms of the yearly averaged DT (Fig. 5c), the DT maxima coincide with the known front positions; in contrast, not all detected fronts show particle accumulation. There are also some differences from the analysis of Pietrzak et al. (2011), who analysed the dynamics of the Frisian Front and East Anglia Plume using satellite data of the sea surface temperature (SST) and suspended particulate matter (SPM). The differences between the present simulations and the results of

https://doi.org/10.5194/os-2019-123
Preprint. Discussion started: 9 December 2019

Ocean Science
Discussions

Pietrzak et al. (2011) in the East Anglia Plume are mostly because the particles in the model have a neutral buoyancy and because no particle sources are prescribed (the seeding is uniform).

To demonstrate the ability of a front to accumulate particles, a surface section across the Rhine Plume (Frisian Front) is chosen as an example (solid black line in Fig. 5a; see also its inset). The front separates the waters of the English Channel (higher salinity) and the Rhine ROFI (lower salinity). In Fig. 7, the graphs start in the west (left) and end in the east (right). The maximum DT in the CR (left vertical dashed line) is located where the salinity and temperature start to decrease (~34.5 to 28.7 PSU and ~12.7 to 11.1°C, respectively). The related density changes are ~4.51 and ~0.30 kg m^{-3}. Hence, the salinity causes the density gradient which in turn influences the accumulation of particles. In the backward simulation (CR-B), the DT maximum (right vertical dashed line; experiment #3, see Table 2) is at the same location with respect to the salinity change when the particles are coming from the opposite direction (forward: southwest, backward: northeast). The peaks of the DT curves are bounded by a rather constant DT, which is higher on the side of particle supply than on the side of particle dispersion in CR. In CR-B the particle supply is hampered by the front. These results are very similar to what has been suggested by Lohmann and Belkin (2014) (see their Fig. 2). Despite the vertical dynamics (see Sect. 3.3), particle accumulation along fronts can be explained considering that the mean velocity is not parallel to the front but oriented further clockwise (in the CR the orientation of the front is almost in the north–south direction, whereas U is veered clockwise). This would lead to a crossing of the front by particles, but the particles are hindered by the (haline) front and flow along it. In the CR-B, the dynamics are reversed, and thus, particles accumulate on the other side of the front. Particle accumulation along other ROFIs can also be observed at, e.g. the western Danish coast along the Elbe River outflow. Postma (1984) called the boundary of the Wadden Sea a “line of no return” whose location is comparable to a strong salinity gradient (Fig. 2c and 2d). From the results of the present study, this interpretation of the boundary of the Wadden Sea can be confirmed: if a particle of the German Bight crosses the front, it is unlikely that it will be able to return.

https://doi.org/10.5194/os-2019-123
Preprint. Discussion started: 9 December 2019

Ocean Science
Discussions
Open Access

In the NWE (Fig. 6e), the Frisian and Irish Sea Fronts are less pronounced than in the CR, demonstrating the intensification of frontal accumulation by wind. Due to the missing westerly wind, particles are no longer transported to the fronts, where they can accumulate in the areas of thermohaline gradients. This is especially true for regions where the wind is constantly blowing in the same direction, e.g. regions within the westerlies.

Another kind of shelf front is a tidal mixing front (Sect. 2.3 and Fig. S2), whose dynamics have been described repeatedly (e.g. Hill et al., 1993). These fronts are known to accumulate natural and artificial flotsam (Simpson and Pingree, 1978). Analyses of the January NTE results do not reveal that the DT maxima disappear if the tides are turned off. In July, tidal mixing fronts are clearly visible as temperature gradients (Fig. S2a), and some of them can be observed in terms of DT patterns (Fig. S2c). In contrast to January, these fronts disappear in July if the tides are turned off (Fig. S2d). Due to their seasonal occurrence, these tidal mixing fronts are less pronounced in the yearly averaged DT then others are, e.g. the fronts of ROFIs. However, not all tidal mixing fronts occur as DT maxima. Although the well-known jet-like velocities along fronts can be seen in U in Fig. 7, the horizontal model resolution is possibly too coarse; that is, the model cannot resolve all important frontal dynamics.

3.3. Vertical circulation in the North Sea

Although shelf dynamics are dominated by strong horizontal motions, they cannot be considered fully two-dimensional. Examples of the role of vertical processes are given by tidal mixing fronts (Garret and Loder, 1981; van Aken et al, 1987), upwelling in the German Bight (Krause et al., 1986), tidal straining (de Boer et al., 2009) and secondary circulation in estuaries. The differences between the surface and bottom accumulation patterns described in Sect. 3.2.4 (Fig. 5a and 5b) are indicative of the role of vertical processes. Such indications are clearly observed in the map of the differences between the vertical positions of particles released at the bottom after one month of integration (Fig. 8a). These differences are very pronounced along the eastern British coast, eastern Irish coast, around the Dogger Bank and in several smaller coastal areas, e.g. at the western French coast. Some of these patterns are topographically induced, like the one at the Dogger Bank, where particles from the northwest ascend

https://doi.org/10.5194/os-2019-123
Preprint. Discussion started: 9 December 2019

and particles released on the Dogger Bank descend. However, a DT at the surface smaller than 1 and a DT at the bottom greater than 1 (compare Fig. 5c with 5d) suggest an upward movement of water. Single particle trajectories along the British coast reveal that the bottom flow is directed coastward and offshore at the surface (small inset in Fig. 8a). Locations with dominant upwelling or downwelling are indicated with "↑" and "↓" symbols, respectively, in Fig. 8a.

In the backtracking experiment (CR-B, experiment #3, see Table 2; Fig. 8b), particles accumulate in coastal upwelling areas, emphasising the dynamics described above. The opposite situation is present on the western Irish coast and in the western Irish Sea; here, a downward movement of water can be observed. The NWE shows that the main driver of coastal water transport at meridionally oriented coasts is the prevailing westerlies (Fig. 6e and 6f). Without wind, the eastern Irish and British coasts have DT values clearly exceeding 0.3; with the original wind forcing, these areas have DT values smaller than 0.3. In contrast, the DT of the western Irish coast and in the western Irish Sea is reduced in the NWE. These results also support the theory of Lentz and Fewings (2012) regarding wind-driven inner-shelf circulation.

Wind forcing is not the only explanation for the offshore-directed transport at some of the shelf coasts, particularly along the eastern British coast. Downwelling at fronts is associated with upwelling on the coastward side as a result of coastward transport at the bottom and offshore-directed transport at the surface. Similar effects have been modelled (Garret and Loder, 1981) and observed (van Aken et al., 1987) in previous investigations.

3.4. Dynamics at the shelf edge

The analysis below uses the results of the CR-V with the seeding prescribed in a 100 km wide segment extending oceanward from the 150 m isobaths (experiment #2, see Table 2). The exchange of particles between the deep ocean and the shelf is estimated by the number of particles crossing the 200 m isobaths and the changes in their depth with respect to the depth at which they were released. The 100 km wide segment is divided vertically into four parts: from the surface to 80 m (Fig. 9a), 100–180 m (Fig. 9b),

https://doi.org/10.5194/os-2019-123
Preprint. Discussion started: 9 December 2019

Ocean Science Discussions
Open Access
EGU

200–280 m (Fig. 9c) and 900–980 m (Fig. 9d). The major result of this experiment is that with increasing depth (1) the dispersion of the cloud of particles in the vicinity of the 200 m isobaths decreases, and (2) particles in the deeper layers do not penetrate onto the shelf. Many particles released above 100 m move onto the shelf; their depth remains almost unchanged or even decreases (Fig. 9a). In the three deeper intervals of release, deep oceanward transport is dominant (red stripe along the 200 m isobath in Fig. 9b, c and d). These dynamics, which are sketched in Fig. 9e, support the results of Holt et al. (2009), Huthnance et al. (2009) and Graham et al (2018), whose simulations also showed shelfward transport distinctive of the upper 150 m along the 200 m isobath; below 150 m, they found deep oceanward transport. The simulated exchanges between the shelf and open ocean (the extent and direction of particle propagation) are also in overall agreement with the recent results of Marsh et al. (2017), who analysed drifter observations and Lagrangian simulations at the ENWS continental slope. Down to 280 m, particles propagating away from the continental slope form filaments or eddy-like patterns as in the Rockall Trough; another fraction of the particles are advected within the slope current. Although the latter are covered by the coloured areas, some of them are visible at the entrance of the Norwegian Trench. The underlying dynamics at the ENWS continental slope are discussed in Sect. 3.2.1.

4 Conclusions

Lagrangian analyses in conjunction with Eulerian analyses revealed physically distinct regimes in different parts of the study area. The underlying dynamics were investigated in terms of particle accumulation and removal, which were quantified by the DT quantity.

- On the shelf: Fronts act as barriers and accumulate particles. Tides affect the positions and appearance of particle accumulation in frontal areas. Vertical water transport at meridionally oriented coasts on the shelf is influenced by westerlies. Offshore-directed wind induces a DT smaller than 1; the situation is reversed for onshore-directed wind.
- In the deep ocean: Eddies influence the particle dynamics on short time scales (individual months); however, an annual mean DT ≈ 1 reveals an absence of long-term stable accumulation areas. Tides affect the DT, suggesting the interaction of tides and mesoscale dynamics.

- Shelf edge (200 m isobath): The shelf edge represents a transition zone from the wind- and tidally driven shallow shelf regime to a baroclinic eddy-dominated deep ocean regime. The shelf edge shows on-shelf transport in the upper layers and downwelling-like off-shelf-directed transport below 100 m. Bottom current branches tend to remove particles from the continental slope.
- At the surface: Accumulation patterns on the shelf show high variability on monthly time scales; some accumulation areas remain stable on yearly time scales. These long-term stable zones occur mainly along the fronts of ROFIs and in the Skagerrak. At the shelf edge, particles are transported onto the shelf by westerlies. The influence of wind on particle accumulation is on the order of the influence of tides.
- At the bottom: On the shelf, bottom currents are mainly influenced by the topography and follow its thalweg.

The differences in the properties of the velocity field (e.g. deformation) reveal two different regimes: a shelf regime with rather little deformation and a deep ocean regime with considerable deformation. On the shelf, tidally induced deformation plays a substantial role in particle accumulation and dispersal.

The present study demonstrates the illustrative potential of Lagrangian methods. In conjunction with traditional Eulerian analysis, Lagrangian analysis can enhance the interpretation of observed or simulated dynamics and provide a solid basis for estimating the propagation of floating marine debris.

Code/data availability: The model codes of NEMO, ARIANE and OpenDrift as well as the GPS drifter and HF radar data are freely available. Scripts and data can be obtained by a request to the corresponding author.

Author contributions. MR and EVS conceived the study. MR performed the model runs and analysed and prepared the figures. MR and EVS interpreted the results, and MR prepared the manuscript with a significant contribution from EVS.

Competing interests. The authors declare that they have no conflicts of interest.

Acknowledgments. We thank the UK Met Office and Joanna Staneva for providing the NEMO AMM7 setup. This study was carried out within the project "Macroplastics Pollution in the Southern North Sea – Sources, Pathways and Abatement Strategies" (grant no. ZN3176) funded by the German Federal State of Lower Saxony. The authors thank Sebastian Grayek for technical support and Jens Meyerjürgens for carefully reading the manuscript and giving important advice.

References

van Aken, H. M. (2001). The hydrography of the mid-latitude Northeast Atlantic Ocean — Part III: the subducted thermocline water mass. *Deep Sea Res. Pt. I: Oceanographic Research Papers*, *48*(1), 237–267. https://doi.org/10.1016/S0967-0637(00)00059-5

van Aken, H. M., van Heijst, G. J. F., & Maas, L. R. M. (1987). Observations of fronts in the North Sea. *J. Mar. Res.*, *45*(3), 579–600. https://doi.org/10.1357/002224087788326830

Backhaus, J. (1979). First Results of a Three-Dimensional Model on the Dynamics in the German Bighta. In J. C. J. Nihoul (Ed.), *Elsev. Oceanogr. Serie.* (Vol. 25, pp. 333–349). Elsevier. https://doi.org/10.1016/S0422-9894(08)71138-3

Backhaus, J. O. (1985). A three-dimensional model for the simulation of shelf sea dynamics. *Deutsche Hydrografische Zeitschrift*, *38*(4), 165–187. https://doi.org/10.1007/BF02328975

Baschek, B., Schroeder, F., Brix, H., Riethmuller, R., Badewien, T.H., Breitbach, G., et al. (2017). The coastal observing system for northern and arctic seas (COSYNA). Ocean Sci. *13*(3), 379–410. https://doi.org/10.5194/os-13-379-2107

https://doi.org/10.5194/os-2019-123
Preprint. Discussion started: 9 December 2019

Ocean Science Discussions

Belkin, I. M., Cornillon, P. C., & Sherman, K. (2009). Fronts in Large Marine Ecosystems. *Prog. Oceanogr.*, *81*(1), 223–236. https://doi.org/10.1016/j.pocean.2009.04.015

Beron-Vera, F. J., Hadjighasem, A., Xia, Q., Olascoaga, M. J., & Haller, G. (2018). Coherent Lagrangian swirls among submesoscale motions. *P. Natl. Acad. Sci. USA*, 201701392. https://doi.org/10.1073/pnas.1701392115

Blanke, B., & Raynaud, S. (1997). Kinematics of the Pacific Equatorial Undercurrent: An Eulerian and Lagrangian Approach from GCM Results. *J. Phys. Oceanogr.*, *27*(6), 1038–1053. https://doi.org/10.1175/1520-0485(1997)027<1038:KOTPEU>2.0.CO;2

Blanke, B., Arhan, M., Madec, G., & Roche, S. (1999). Warm Water Paths in the Equatorial Atlantic as Diagnosed with a General Circulation Model. *J. Phys. Oceanogr.*, *29*(11), 2753–2768. https://doi.org/10.1175/1520-0485(1999)029<2753:WWPITE>2.0.CO;2

de Boer, G. J., Pietrzak, J. D., & Winterwerp, J. C. (2009). SST observations of upwelling induced by tidal straining in the Rhine ROFI. *Cont. Shelf Res.*, *29*(1), 263–277. https://doi.org/10.1016/j.csr.2007.06.011

Booth, D. A. (1988). Eddies in the Rockall Trough. *Oceanologica Acta*, *11*(3), 213–219.

Bower, A. S., Lozier, M. S., Gary, S. F., & Böning, C. W. (2009). Interior pathways of the North Atlantic meridional overturning circulation. *Nature*, *459*(7244), 243–247. https://doi.org/10.1038/nature07979

Brown, J., Hill, A. E., Fernand, L., & Horsburgh, K. J. (1999). Observations of a Seasonal Jet-like Circulation at the Central North Sea Cold Pool Margin. *Estuar. Coast. Shelf S.*, *48*(3), 343–355. https://doi.org/10.1006/ecss.1999.0426

Brown, J., Carrillo, L., Fernand, L., Horsburgh, K. J., Hill, A. E., Young, E. F., & Medler, K. J. (2003). Observations of the physical structure and seasonal jet-like circulation of the Celtic Sea and St. George's Channel of the Irish Sea. *Cont.l Shelf Res.*, *23*(6), 533–561. https://doi.org/10.1016/S0278-4343(03)00008-6

Callies, U., Plüß, A., Kappenberg, J., & Kapitza, H. (2011). Particle tracking in the vicinity of Helgoland, North Sea: a model comparison. *Ocean Dynam.*, *61*(12), 2121–2139. https://doi.org/10.1007/s10236-011-0474-8

https://doi.org/10.5194/os-2019-123
Preprint. Discussion started: 9 December 2019

Carrasco, R., & Horstmann, J. (2017). *German Bight surface drifter data from Heincke cruise HE 445, 2015*, PANGAEA. https://doi.org/10.1594/PANGAEA.874511

Daewel, U., Peck, M. A., Kühn, W., St. John, M. A., Alekseeva, I., & Schrum, C. (2008). Coupling ecosystem and individual-based models to simulate the influence of environmental variability on potential growth and survival of larval sprat (Sprattus sprattus L.) in the North Sea. *Fish. Oceanogr.*, *17*(5), 333–351. https://doi.org/10.1111/j.1365-2419.2008.00482.x

Dagestad, K.-F., Röhrs, J., Breivik, Ø., & Ådlandsvik, B. (2017). OpenDrift v1.0: a generic framework for trajectory modeling. *Geosci. Model Dev.*, *2017*, 1–28. https://doi.org/10.5194/gmd-2017-205

Davies, A. M, & Xing, J. (2001). Modelling processes influencing shelf edge currents, mixing, across shelf exchange, and sediment movement at the shelf edge. *Dynam. Atmos. Oceans*, *34*(2), 291–326. https://doi.org/10.1016/S0377-0265(01)00072-0

Davies, A. M., Sauvel, J., & Evans, J. (1985). Computing near coastal tidal dynamics from observations and a numerical model. *Cont. Shelf Res.*, *4*(3), 341–366. https://doi.org/10.1016/0278-4343(85)90047-0

Froyland, G., Stuart, R. M., & van Sebille, E. (2014). How well-connected is the surface of the global ocean? *Chaos*, *24*(3), 033126. https://doi.org/10.1063/1.4892530

Garrett, C. J. R., & Loder, J. W. (1981). Circulation and fronts in continental shelf seas - Dynamical aspects of shallow sea fronts. *Philos. T. Roy. Soc. A*, *302*(1472), 563–581. https://doi.org/10.1098/rsta.1981.0183

Graham, J. A., Rosser, J. P., O'Dea, E., & Hewitt, H. T. (2018). Resolving Shelf Break Exchange Around the European Northwest Shelf. *Geophysical Research Letters*, *45*(22), 12,386-12,395. https://doi.org/10.1029/2018GL079399

Guihou, K., Polton, J., Harle, J., Wakelin, S., O'Dea, E., & Holt, J. (2018). Kilometric Scale Modeling of the North West European Shelf Seas: Exploring the Spatial and Temporal Variability of Internal Tides. *J. Geophys. Res.-Oceans*, *122*. https://doi.org/10.1002/2017JC012960

Gutow, L., Ricker, M., Holstein, J., Dannheim, J., Stanev, E. V. & Wolff, J.-O. (2018). Distribution and trajectories of floating and benthic marine macrolitter in the south-eastern North Sea. *Mar. Pollut. Bull.*, *131*, *Part A*, 763–772. https://doi.org/10.1016/j.marpolbul.2018.05.003

Hainbucher, D., Pohlmann, T., & Backhaus, J. (1987). Transport of conservative passive tracers in the North Sea: first results of a circulation and transport model. *Cont. Shelf Res.*, *7*(10), 1161–1179. https://doi.org/10.1016/0278-4343(87)90083-5

Haller, G., & Yuan, G. (2000). Lagrangian coherent structures and mixing in two-dimensional turbulence. *Physica D*, *147*(3), 352–370. https://doi.org/10.1016/S0167-2789(00)00142-1

Heaps, N. S. (1980). Density currents in a two-layered coastal system, with application to the Norwegian Coastal Current. *Geophys. J. Roy. Astr. S.*, *63*(2), 289–310. https://doi.org/10.1111/j.1365-246X.1980.tb02622.x

Hill, A. E., James, I. D., Linden, P. F., Matthews, J. P., Prandle, D., Simpson, J. H., et al. (1993). Understanding the North Sea system - Dynamics of tidal mixing fronts in the North Sea. *Philos. T. Roy. Soc. A*, *343*(1669), 431–446. https://doi.org/10.1098/rsta.1993.0057

Hill, A. E., Brown, J., Fernand, L., Holt, J., Horsburgh, K. J., Proctor, R., Raine, R., & Turrell, W. R. (2008). Thermohaline circulation of shallow tidal seas. *Geophys. Res. Lett.*, *35*(11), L11605. https://doi.org/10.1029/2008GL033459

Holmström, A. (1975). Plastic films on the bottom of the Skagerack. *Nature*, *255*(5510), 622–623. https://doi.org/10.1038/255622a0

Holt, J. T., & James, I. D. (1999). A simulation of the Southern North Sea in comparison with measurements from the North Sea Project. Part 1: Temperature. *Cont. Shelf Res.*, *19*(8), 1087–1112. https://doi.org/10.1016/S0278-4343(99)00015-1

Holt, J., & Umlauf, L. (2008). Modelling the tidal mixing fronts and seasonal stratification of the Northwest European Continental shelf. *Cont. Shelf Res.*, *28*(7), 887–903. https://doi.org/10.1016/j.csr.2008.01.012

Holt, J., Wakelin, S., & Huthnance, J. (2009). Down-welling circulation of the northwest European continental shelf: A driving mechanism for the continental shelf carbon pump. *Geophysical Research Letters*, *36*(14), L14602. https://doi.org/10.1029/2009GL038997

https://doi.org/10.5194/os-2019-123
Preprint. Discussion started: 9 December 2019

Huntley, H. S., Lipphardt, B. L., Jacobs, G., & Kirwan, A. D. (2015). Clusters, deformation, and dilation: Diagnostics for material accumulation regions. *Journal of Geophysical Research: Oceans*, *120*(10), 6622–6636. https://doi.org/10.1002/2015JC011036

Huthnance, J. M. (1991). Physical oceanography of the North Sea. *Ocean and Shoreline Management*, *16*(3), 199–231. https://doi.org/10.1016/0951-8312(91)90005-M

Huthnance, J. M. (1995). Circulation, exchange and water masses at the ocean margin: the role of physical processes at the shelf edge. *Prog. Oceanogr., 35*(4), 353–431. https://doi.org/10.1016/0079-6611(95)80003-C

Huthnance, J. M., Holt, J. T., & Wakelin, S. L. (2009). Deep ocean exchange with west-European shelf seas. *Ocean Sci.*, *5*(4), 621–634. https://doi.org/10.5194/os-5-621-2009

Jacob, B., & Stanev, E. V. (2017). Interactions between wind and tidally induced currents in coastal and shelf basins. *Ocean Dynam.*, *67*(10), 1263–1281. https://doi.org/10.1007/s10236-017-1093-9

Jacobs, G. A., Huntley, H. S., Kirwan, A. D., Lipphardt, B. L., Campbell, T., Smith, T., Edwards, K., & Bartels, B. (2016). Ocean processes underlying surface clustering. *J. Geophys. Res. Oceans*, *121*(1), 180–197. https://doi.org/10.1002/2015JC011140

Krause, G., Budeus, G., Gerdes, D., Schaumann, K., & Hesse, K. (1986). Frontal Systems in the German Bight and their Physical and Biological Effects. In J. C. J. Nihoul (Ed.), *Elsev. Oceanogr. Serie.* (Vol. 42, pp. 119–140). Elsevier. https://doi.org/10.1016/S0422-9894(08)71042-0

Koszalka, I. M., & LaCasce, J. H. (2010). Lagrangian analysis by clustering. *Ocean Dynamics*, *60*(4), 957–972. https://doi.org/10.1007/s10236-010-0306-2

Koszalka, I. M., LaCasce, J. H., Andersson, M., Orvik, K. A., & Mauritzen, C. (2011). Surface circulation in the Nordic Seas from clustered drifters. *Deep Sea Research Part I: Oceanographic Research Papers*, *58*(4), 468–485. https://doi.org/10.1016/j.dsr.2011.01.007

Le Fèvre, J. (1986). Aspects of the Biology of Frontal Systems. *Adv. Mar. Biol.*, *23*, 163–299.

Lentz, S. J., & Fewings, M. R. (2012). The wind- and wave-driven inner-shelf circulation. *Annu. Rev. Mar. Sci.*, *4*(1), 317–343. https://doi.org/10.1146/annurev-marine-120709-142745

Lohmann, R., & Belkin, I. M. (2014). Organic pollutants and ocean fronts across the Atlantic Ocean: A review. *Prog. Oceanogr.*, *128*(Supplement C), 172–184. https://doi.org/10.1016/j.pocean.2014.08.013

Madec, G. (2008). NEMO ocean engine. *Note du Pôle de modélisation, Institut Pierre-Simon Laplace (IPSL), France*, (27).

Mahadevan, A. (2016). The Impact of Submesoscale Physics on Primary Productivity of Plankton. *Annu. Rev. Mar. Sci.*, *8*, 161–184. https://doi.org/10.1146/annurev-marine-010814-015912

Maier-Reimer, E. (1977). Residual circulation in the North Sea due to the M2-tide and mean annual wind stress. *Deutsche Hydrografische Zeitschrift*, *30*(3), 69–80. https://doi.org/10.1007/BF02227045

Marsh, R., Haigh, I. D., Cunningham, S. A., Inall, M. E., Porter, M., & Moat, B. I. (2017). Large-scale forcing of the European Slope Current and associated inflows to the North Sea. *Ocean Sci.*, *13*(2), 315–335. https://doi.org/10.5194/os-13-315-2017

Maximenko, N., Hafner, J., Kamachi, M., & MacFadyen, A. (2018). Numerical simulations of debris drift from the Great Japan Tsunami of 2011 and their verification with observational reports. *Mar. Pollut. Bull.*, *132*, 5–25. https://doi.org/10.1016/j.marpolbul.2018.03.056

McWilliams, J. C. (2016). Submesoscale currents in the ocean. *P. Roy. Soc. A-Math. Phy.*, *472*(2189), 20160117. https://doi.org/10.1098/rspa.2016.0117

van der Molen, J., García-García, L. M., Whomersley, P., Callaway, A., et al. (2018). Connectivity of larval stages of sedentary marine communities between hard substrates and offshore structures in the North Sea. *Scientific Reports*, *8*(1), 14772. https://doi.org/10.1038/s41598-018-32912-2

Molinari, R., & Kirwan, A. D. (1975). Calculations of Differential Kinematic Properties from Lagrangian Observations in the Western Caribbean Sea. *J. Phys. Oceanogr.*, *5*(3), 483–491. https://doi.org/10.1175/1520-0485(1975)005<0483:CODKPF>2.0.CO;2

Neumann, D., Callies, U., & Matthies, M. (2014). Marine litter ensemble transport simulations in the southern North Sea. *Mar. Pollut. Bull.*, *86*(1), 219–228. https://doi.org/10.1016/j.marpolbul.2014.07.016

https://doi.org/10.5194/os-2019-123
Preprint. Discussion started: 9 December 2019

O'Dea, E. J., Arnold, A. K., Edwards, K. P., Furner, R., Hyder, P., Martin, M. J., Siddorn, J. R., et al. (2012). An operational ocean forecast system incorporating NEMO and SST data assimilation for the tidally driven European North-West shelf. *J. Oper. Oceanogr.*, *5*(1), 3–17. https://doi.org/10.1080/1755876X.2012.11020128

O'Dea, E. J., Furner, R., Wakelin, S., Siddorn, J., While, J., Sykes, P., et al. (2017). The CO5 configuration of the 7 km Atlantic Margin Model: large-scale biases and sensitivity to forcing, physics options and vertical resolution. *Geosci. Model Dev.*, *10*(8), 2947–2969. https://doi.org/10.5194/gmd-10-2947-2017

Onink, V., Wichmann, D., Delandmeter, P., & Van Sebille, E. (n.d.). The Role of Ekman Currents, Geostrophy, and Stokes Drift in the Accumulation of Floating Microplastic. *J. Geophys. Res.-Oceans*, *124*(3), 1474–1490. https://doi.org/10.1029/2018JC014547

Otto, L., Zimmerman, J. T. F., Furnes, G. K., Mork, M., Saetre, R., & Becker, G. (1990). Review of the physical oceanography of the North Sea. *Neth. J. Sea Res.*, *26*(2), 161–238. https://doi.org/10.1016/0077-7579(90)90091-T

Paparella, F., Babiano, A., Basdevant, C., Provenzale, A., & Tanga, P. (1997). A Lagrangian study of the Antarctic polar vortex. *J. Geophys. Res.-Atmos.*, *102*(D6), 6765–6773. https://doi.org/10.1029/96JD03377

Pätsch, J., Burchard, H., Dieterich, C., Gräwe, U., Gröger, M., Mathis, M., et al. (2017). An evaluation of the North Sea circulation in global and regional models relevant for ecosystem simulations. *Ocean Model.*, *116*(Supplement C), 70–95. https://doi.org/10.1016/j.ocemod.2017.06.005

Pietrzak, J. D., de Boer, G. J., & Eleveld, M. A. (2011). Mechanisms controlling the intra-annual mesoscale variability of SST and SPM in the southern North Sea. *Cont. Shelf Res.*, *31*(6), 594–610. https://doi.org/10.1016/j.csr.2010.12.014

Pingree, R. D., & Griffiths, D. K. (1978). Tidal fronts on the shelf seas around the British Isles. *J. Geophys. Res.-Oceans*, *83*(C9), 4615–4622. https://doi.org/10.1029/JC083iC09p04615

https://doi.org/10.5194/os-2019-123
Preprint. Discussion started: 9 December 2019

Pohlmann, T. (2006). A meso-scale model of the central and southern North Sea: Consequences of an improved resolution. *Cont. Shelf Res.*, *26*(19), 2367–2385. https://doi.org/10.1016/j.csr.2006.06.011

Porter, M., Inall, M. E., Green, J. A. M., Simpson, J. H., Dale, A. C., & Miller, P. I. (2016). Drifter observations in the summer time Bay of Biscay slope current. *Journal of Marine Systems*, *157*, 65–74. https://doi.org/10.1016/j.jmarsys.2016.01.002

Postma, H. (1984). Introduction to the symposium on organic matter in the Wadden Sea. In R. W. P. M. Laane & W. J. Wolff (Eds.), *The role of organic matter in the Wadden Sea* (pp. 15–22). Texel, Netherlands.

Reisser, J., Shaw, J., Wilcox, C., Hardesty, B. D., Proietti, M., Thums, M., & Pattiaratchi, C. (2013). Marine Plastic Pollution in Waters around Australia: Characteristics, Concentrations, and Pathways. *PLOS ONE*, *8*(11), e80466. https://doi.org/10.1371/journal.pone.0080466

Rodhe, J. (1987). The large-scale circulation in the Skagerrak; interpretation of some observations. *Tellus A*, *39A*(3), 245–253. https://doi.org/10.1111/j.1600-0870.1987.tb00305.x

Rolinski, S. (1999). On the dynamics of suspended matter transport in the tidal river Elbe: Description and results of a Lagrangian model. *J. Geophys. Res.-Oceans*, *104*(C11), 26043–26057. https://doi.org/10.1029/1999JC900230

Schönfeld, W. (1995). Numerical simulation of the dispersion of artificial radionuclides in the English Channel and the North Sea. *J. Marine Syst.*, *6*(5), 529–544. https://doi.org/10.1016/0924-7963(95)00022-H

van Sebille, E., England, M. H., & Froyland, G. (2012). Origin, dynamics and evolution of ocean garbage patches from observed surface drifters. *Environmental Research Letters*, *7*(4), 044040. https://doi.org/10.1088/1748-9326/7/4/044040

van Sebille, E., Wilcox, C., Lebreton, L., Maximenko, N., Hardesty, B. D., van Franeker, J. A., et al. (2015). A global inventory of small floating plastic debris. *Environmental Research Letters*, *10*(12), 124006. https://doi.org/10.1088/1748-9326/10/12/124006

https://doi.org/10.5194/os-2019-123
Preprint. Discussion started: 9 December 2019

van Sebille, E., Griffies, S. M., Abernathey, R., Adams, T. P., Berloff, P., Biastoch, A., Blanke, B., et al. (2018). Lagrangian ocean analysis: Fundamentals and practices. *Ocean Model.*, *121*, 49–75. https://doi.org/10.1016/j.ocemod.2017.11.008

Simpson, J. H., & Hunter, J. R. (1974). Fronts in the Irish Sea. *Nature*, *250*(5465), 404–406. https://doi.org/10.1038/250404a0

Simpson, J. H., & Pingree, R. D. (1978). Shallow Sea Fronts Produced by Tidal Stirring. In *Oceanic Fronts in Coastal Processes* (pp. 29–42). Berlin: Springer. https://doi.org/10.1007/978-3-642-66987-3_5

Simpson, J. H., & Sharples, J. (2012). *Introduction to the Physical and Biological Oceanography of Shelf Seas*. Cambridge: Cambridge University Press.

Smagorinsky, J. (1963). General circulation experiments with the primitive equations. *Mon. Weather Rev.*, *91*(3), 99–164. https://doi.org/10.1175/1520-0493(1963)091<0099:GCEWTP>2.3.CO;2

Stanev, E. V., Schulz-Stellenfleth, J., Staneva, J., Grayek, S., Grashorn, S., Behrens, A., Koch, W. & Pein, J. (2016). Ocean forecasting for the German Bight: from regional to coastal scales. *Ocean Sci.*, *12*(5), 1105–1136. https://doi.org/10.5194/os-12-1105-2016

Stanev, E. V., Badewien, T. H., Freund, H., Grayek, S., Hahner, F., Meyerjürgens, J., Ricker, M., et al. (2019). Extreme westward surface drift in the North Sea: Public reports of stranded drifters and Lagrangian tracking. *Cont. Shelf Res.*, *177*, 24–32. https://doi.org/10.1016/j.csr.2019.03.003

Stanev, E. V., Ziemer, F., Schulz-Stellenfleth, J., Seemann, J., Staneva, J., & Gurgel, K. W. (2015). Blending Surface Currents from HF Radar Observations and Numerical Modelling: Tidal Hindcasts and Forecasts, *J. Atmos. Ocean. Tech.*, *32*(2), 256–281. https://doi.org/10.1175/JTECH-D-13-00164.1

Wakata, Y., & Sugimori, Y. (1990). Lagrangian Motions and Global Density Distributions of Floating Matter in the Ocean Simulated Using Shipdrift Data. *J. Phys. Oceanogr.*, *20*(1), 125–138. https://doi.org/10.1175/1520-0485(1990)020<0125:LMAGDD>2.0.CO;2

Zhang, Y. J., Stanev, E. V., & Grashorn, S. (2016). Unstructured-grid model for the North Sea and Baltic Sea: Validation against observations. *Ocean Model.*, *97*, 91–108. https://doi.org/10.1016/j.ocemod.2015.11.009

Figure captions:

Fig. 1. Bathymetry of the model domain. The shelf is defined as depths shallower than 200 m (colour bar within the map). In this and all following figures, the 200 m depth contour is highlighted with a black solid line. The abbreviations used in the text are as follows: Armorican Shelf (*AS*), Bay of Biscay (*BB*), Celtic Sea (*CS*), Dogger Bank (*DB*), East Anglia (*EA*), English Channel (*EC*), German Bight (*GB*), Goban Spur (*GS*), Irish Sea (*IS*), Kattegat (*Ka*), North Sea (*NS*), Norwegian Trench (*NT*), Rockall Trough (*RT*), Skagerrak (*Sk*), Southern Bight (*SB*), St. George's Channel (*SGC*), Orkney/Shetland Islands (*OI*/*SI*), Outer Hebrides (*OH*), Porcupine Bank (*PB*), Fair Isle Current (*a*), European Slope Current (*b*), East Anglia Plume (*c*), Frisian Front (*d*), Rhine River (*1*), Ems River (*2*), Weser River (*3*) and Elbe River (*4*).

Fig. 2. Simulated surface properties in the CR for January 2015: velocity magnitude derived from the averaged u und v velocity components (a), mean velocity magnitude (b), mean salinity (c) and mean temperature (e). Magnitudes of the temperature (d) and salinity (f) gradients as well as the deformation (g) in the CR and the differences between the deformation in the CR and NTE (h) are presented as 25-h averaged fields on 15 January 2015.

Fig. 3. Lagrangian trajectories of every 5th particle after 15 days of integration released on 01 January 2015. Particles are released at the surface (a) and bottom (b) (experiment #1, see Table 2). (c) and (d) are magnified views of the domain showing the trajectories of the first 12 h (c) and 24 h (d) representative of different dynamics: the area of the Armorican Shelf continental slope including tidal ellipses (c) and the circulation in the Skagerrak (d). The trajectory colours are randomly chosen for better visibility. Grey lines are isobaths in 700 m (c) and 400 m steps (d).

Fig. 4. Particle positions after 1 month (a) and (b) and 6 months (c) and (d) released on 01 January 2015 of surface-released (a) and (c) and bottom-released particles (b) and (d) (experiment #1, see Table 2). "+" and "-" symbols represent areas with pronounced particle accumulation and dispersion, respectively; details are given in the text.

https://doi.org/10.5194/os-2019-123
Preprint. Discussion started: 9 December 2019

Fig. 5. Tendencies of accumulation shown as the January mean DT (a) and (b) and the annual mean DT for 2015 (c) and (d) (averages of Fig. S3 and S4, respectively). (a) and (c) correspond to surface-released particles, while (b) and (d) correspond to bottom-released particles (experiment #1, see Table 2). In (a), the solid black line located in the German Bight is the transect shown in Fig. 7 (enlarged in the inset). The numbers in (c) indicate the most pronounced accumulation areas.

Fig. 6. Analysis of the sensitivity experiments with respect to tides and wind. (a) and (b) are the differences between the CR and NTE (experiment #4, see Table 2) in January 2015 at the surface (a) and bottom (b). (c) and (d) are the corresponding differences between the CR and FEW; (e) and (f) are the differences between the CR and NWE. The "*" symbols in (a), (b) and (e) denote pronounced differences; see the text for details.

Fig. 7. Density trend (DT), salinity (S), temperature (T) and velocity vectors (U) at the surface as the means of January 2015 along the transect in the German Bight (solid black line in Fig. 5a). The vertical dotted lines mark the DT maxima of the forward (left one, solid DT line) and backward (right one, dashed DT line) simulations (experiments #1 and 3, respectively, see Table 2).

Fig. 8. Difference of the final depth minus the initial depth of bottom-released particles after 1 month (January) in 2015 (a) (experiment #1, see Table 2). Positive/negative values indicate a depth increase/decrease. The model grid in which a particle was released is coloured depending on its depth change. The small figure shows a magnified view of the British coast with two exemplary bottom (black) and surface (red) trajectories starting at the big dots. The trajectories are detided with a 25-h flowing mean. The "↑" and "↓" symbols denote coastal areas favourable for upward and downward water movements, respectively. Tendencies of accumulation are shown as the January mean DT calculated from the backward simulation CR-B (b) (experiment #3, see Table 2).

https://doi.org/10.5194/os-2019-123
Preprint. Discussion started: 9 December 2019

Fig. 9. Particle positions (purple dots) and particle depth differences with respect to the depth of release in different depth layers (colours) after 1 month (January) in 2015 computed in the CR-V (experiment #2, see Table 2). Details of the seeding strategy can be found in Sect. 2.3. The colour coding shows the difference of the final depth minus the initial particle depth, computed as the mean difference of all particle depths seeded at the same location in the horizontal plane. All particles released in the respective depth range are taken into account. Particles were released in four depth layers: from the surface to 80 m (a), 100–180 m (b), 200–280 m (c) and 900–980 m (d). The dynamics at the continental slope concluded from (a) to (d) are sketched in (e).

https://doi.org/10.5194/os-2019-123
Preprint. Discussion started: 9 December 2019

Ocean Science
Discussions

Figures:

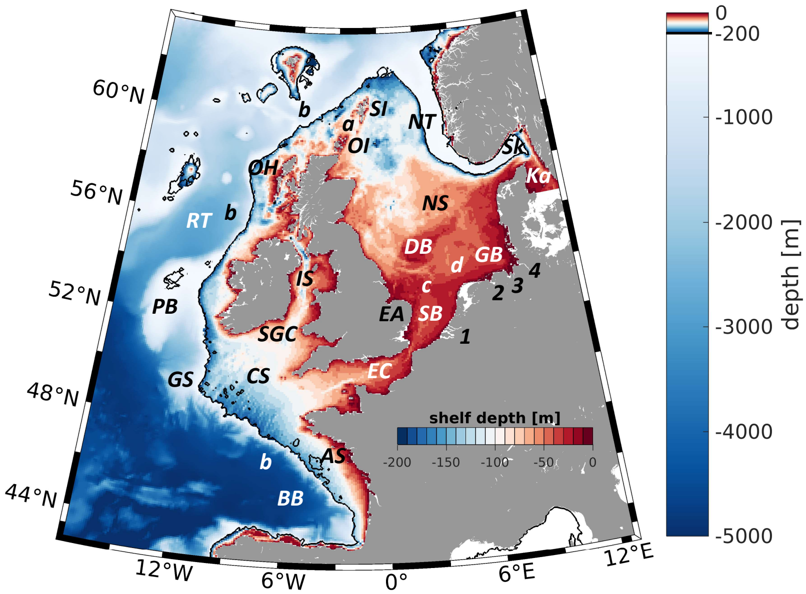

Fig. 1.

https://doi.org/10.5194/os-2019-123
Preprint. Discussion started: 9 December 2019

Ocean Science
Discussions

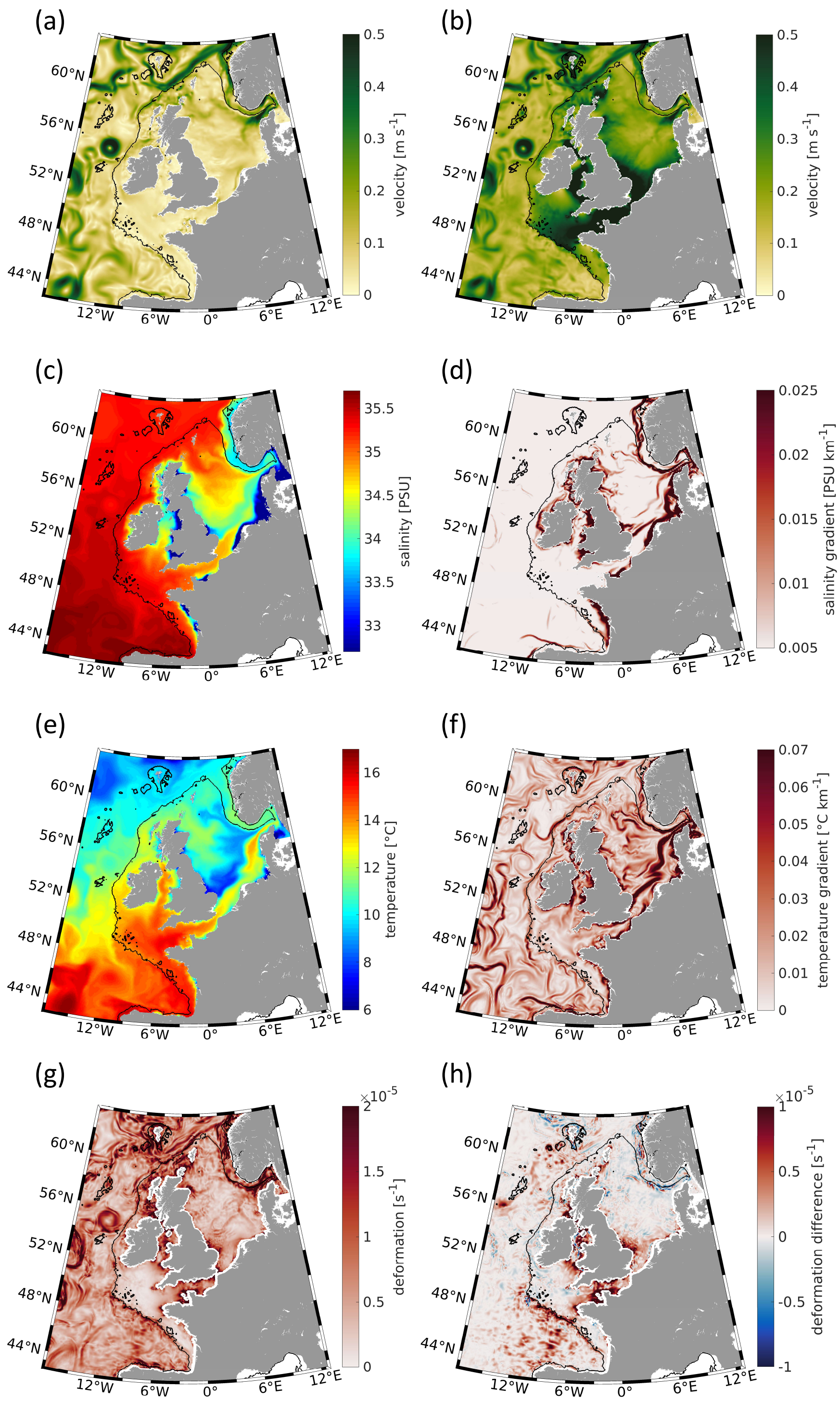

Fig. 2.

https://doi.org/10.5194/os-2019-123
Preprint. Discussion started: 9 December 2019

Ocean Science Discussions
Open Access EGU

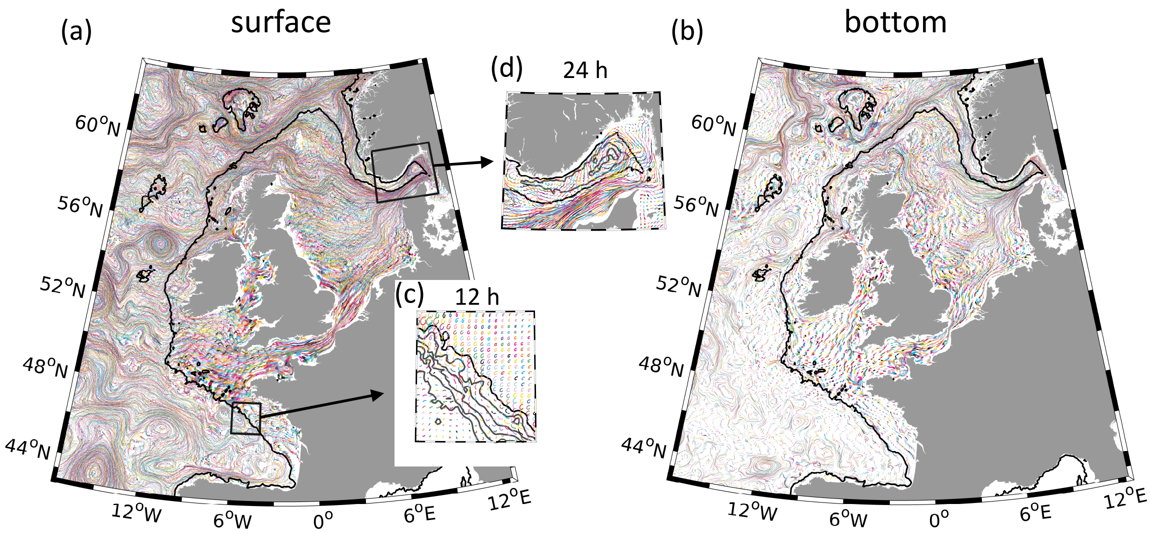

Fig. 3.

https://doi.org/10.5194/os-2019-123
Preprint. Discussion started: 9 December 2019

Ocean Science
Discussions

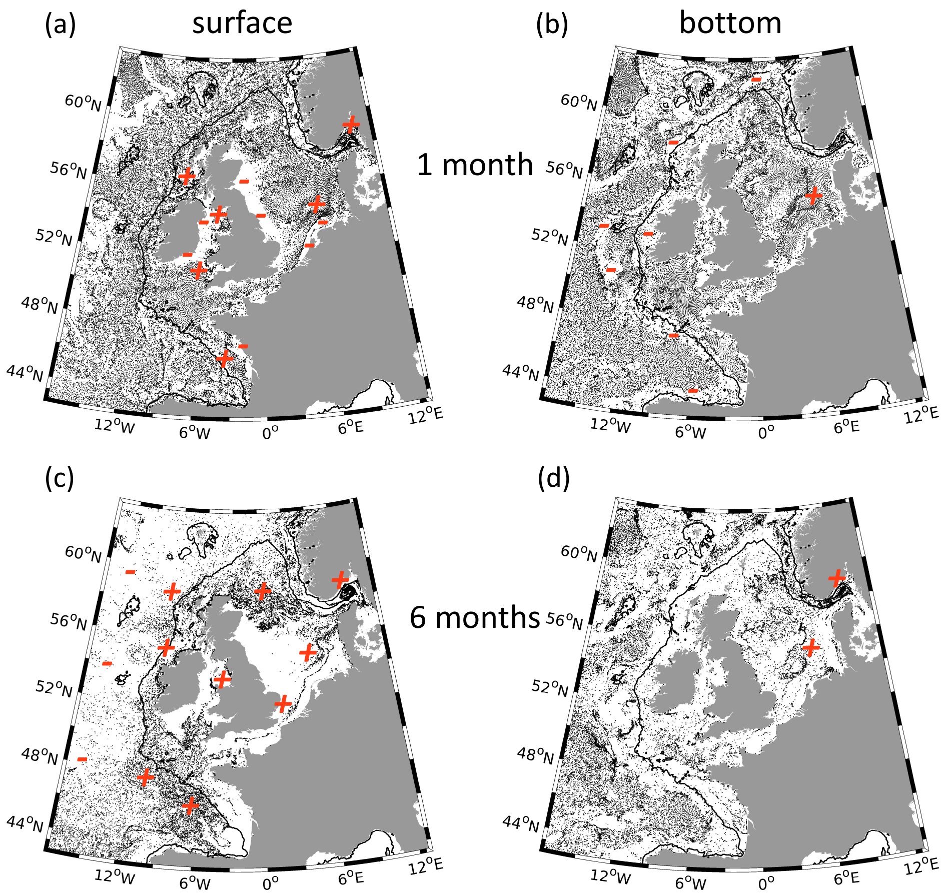

Fig. 4.

https://doi.org/10.5194/os-2019-123
Preprint. Discussion started: 9 December 2019

Ocean Science
Discussions
Open Access

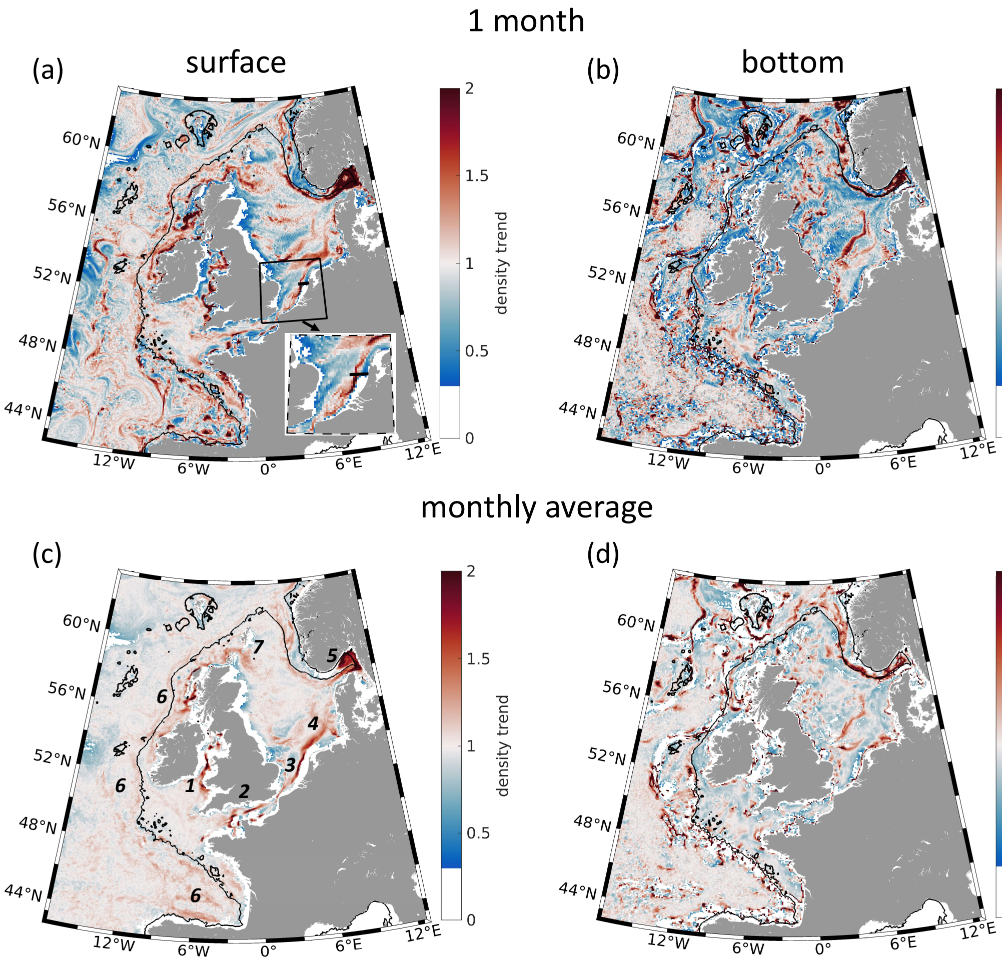

Fig. 5.

https://doi.org/10.5194/os-2019-123
Preprint. Discussion started: 9 December 2019

Ocean Science
Discussions
Open Access

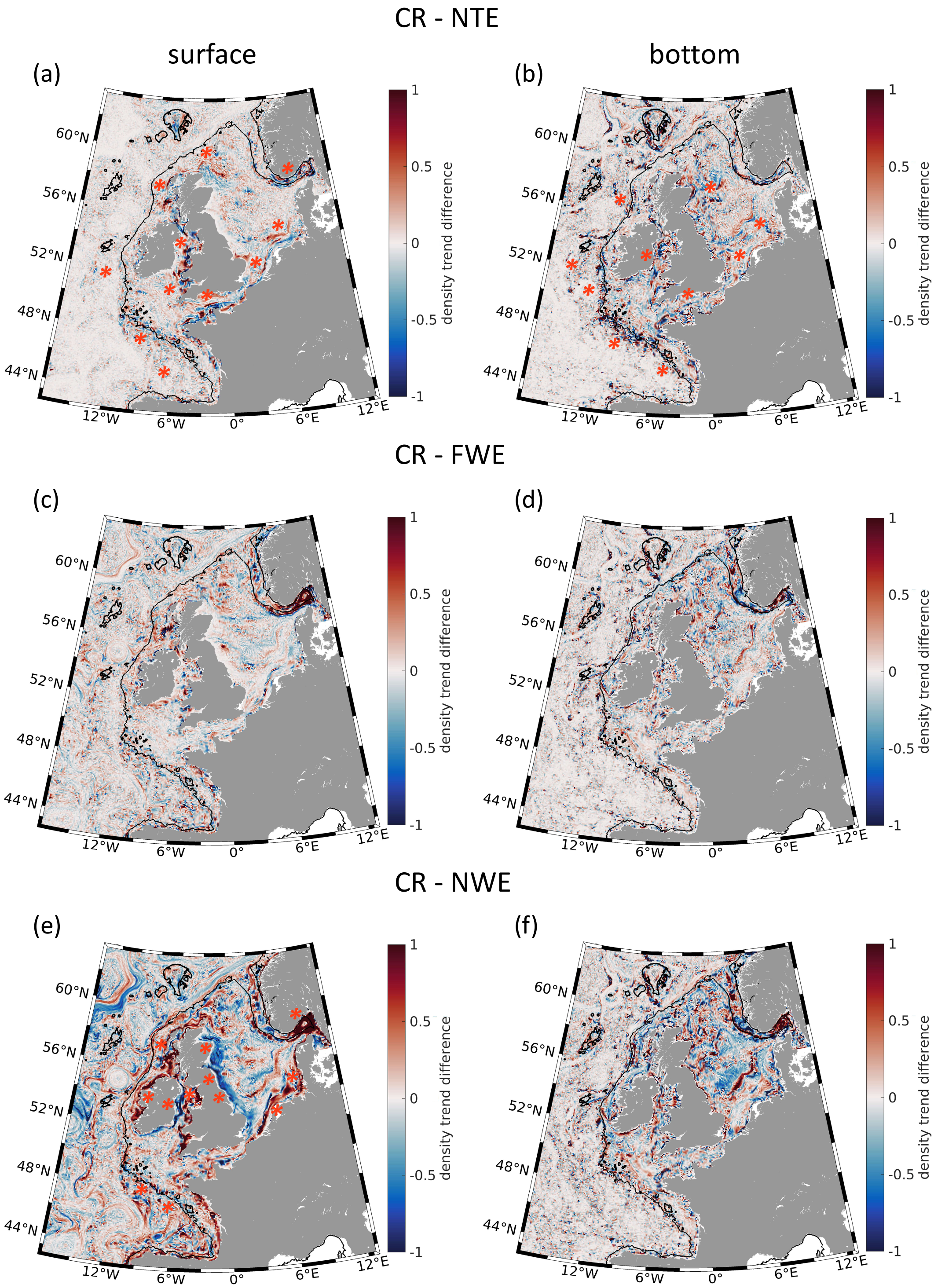

Fig. 6.

https://doi.org/10.5194/os-2019-123
Preprint. Discussion started: 9 December 2019

Ocean Science
Discussions

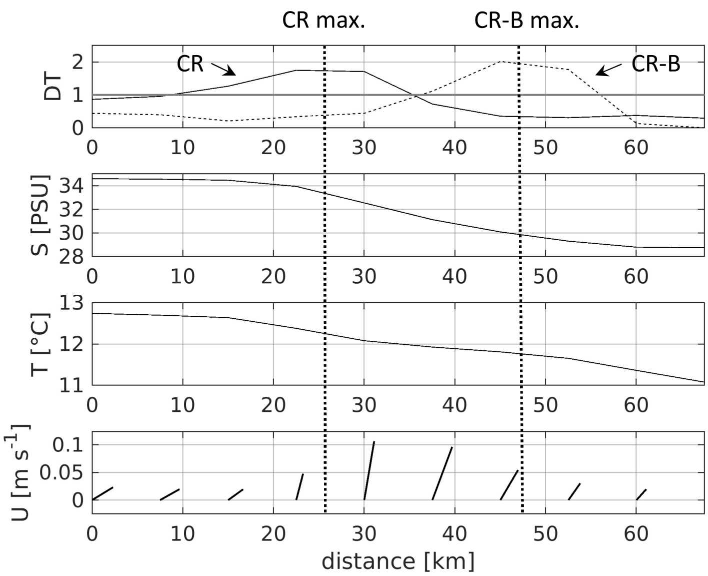

Fig. 7.

https://doi.org/10.5194/os-2019-123
Preprint. Discussion started: 9 December 2019

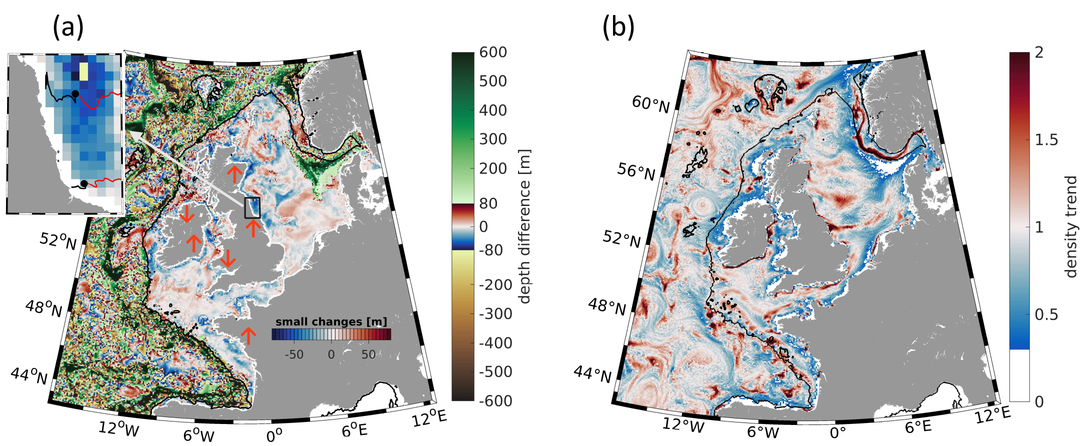

Fig. 8.

https://doi.org/10.5194/os-2019-123
Preprint. Discussion started: 9 December 2019

Ocean Science
Discussions
Open Access
EGU

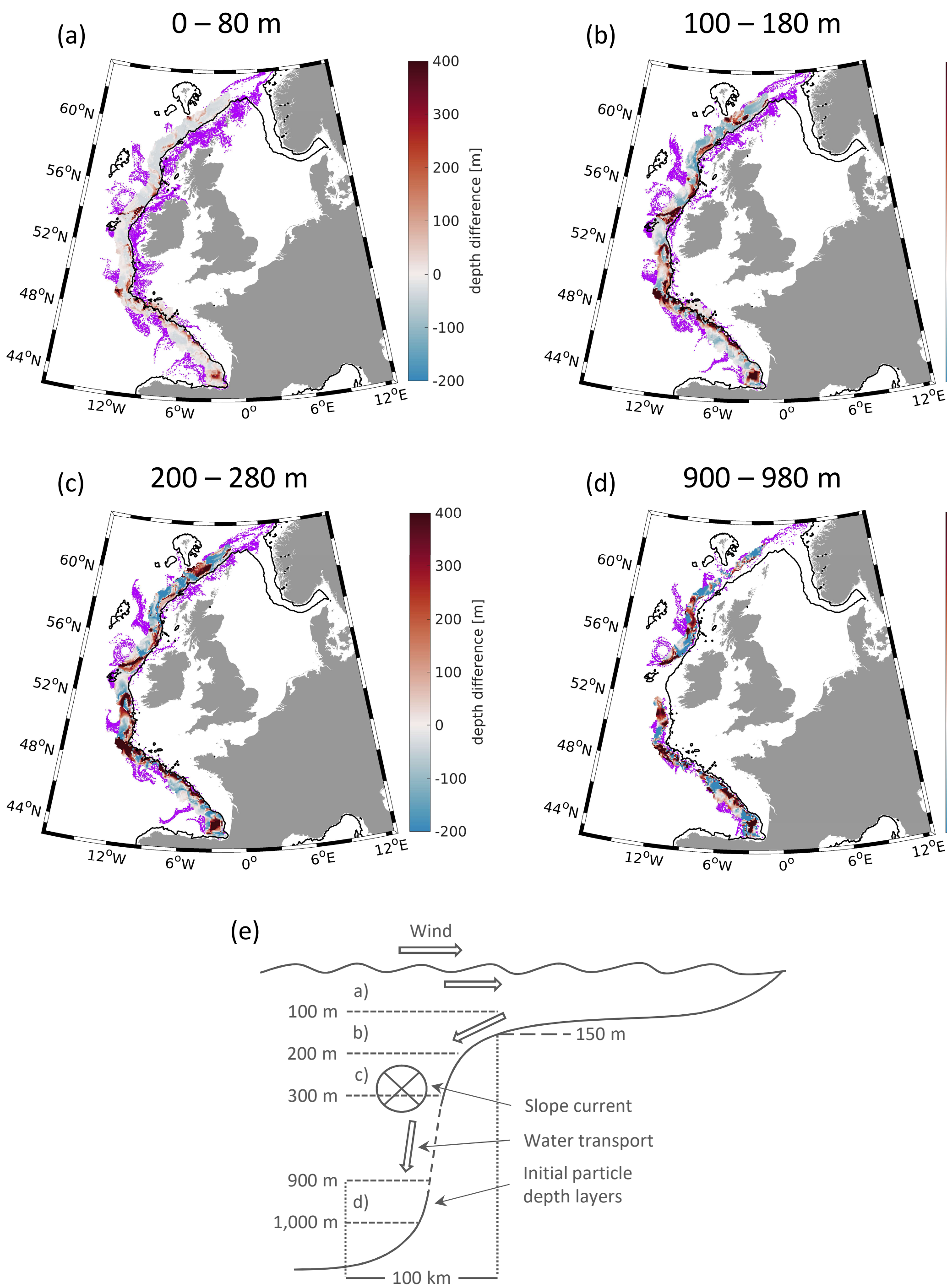

Fig. 9.